3.4 CLOUDSAT'S VIEW OF THE GLOBAL DISTRIBUTION OF LIGHT PRECIPITATION

T. S. L'Ecuyer[1], J. M. Haynes[1], C. Mitrescu[2], F. J. Turk[2], S. D. Miller[2], and C. Kummerow[1]

[1]Colorado State University
Fort Collins, Colorado

[2]Naval Research Laboratory
Monterey, California

ABSTRACT

While significant progress has been made in global precipitation measurement from satellite platforms, the vast majority of current sensors continue to suffer from an inherent lack of sensitivity to light rainfall. Accurate measurements of the distribution of light rain, however, is important for establishing closure of the global water cycle since it represents a significant fraction of total precipitation in many regions particularly those that lie poleward of 40 degrees. By virtue of its sensitivity, the CloudSat Cloud Profiling Radar (CPR), the first millimeter wavelength cloud radar to be flown in space, offers a unique opportunity to perform a global survey of light rainfall and to quantify its contribution to the global water cycle. This presentation will describe the theoretical basis and early validation of an experimental CloudSat precipitation product. Data from CloudSat's first year in orbit will be presented with a primary focus on establishing the global distribution of light rainfall and its spatial and temporal variability. Results will be compared with similar products from established platforms including the Tropical Rainfall Measuring Mission (TRMM) Precipitation Radar and the Advanced Microwave Scanning Radiometer (AMSR-E) aboard Aqua.

1. INTRODUCTION

In spite of recent advances in sensor technology such as the sensors aboard the Tropical Rainfall Measuring Mission (TRMM), there remain several key areas of space-based precipitation retrieval that are not well understood. PMW retrievals that represent the most widely used source of global precipitation information, for example, rely heavily on the lower frequency channels (6-19 GHz, depending on the sensor) where the on-Earth resolutions are the coarsest (e.g. 40 km in the case of TRMM Microwave Imager, TMI). Furthermore, due to the fundamental path-integrated nature of a passive measurement, there is an uncertainty associated with the discrimination of precipitating and non-precipitating cloud. This leads to uncertainty in both the up-front screening of a rain/no-rain pixel(s) and the retrieved intensity. Over land, PMW retrievals are inhibited by the radiometrically warm surface emissivity, which varies widely both spatially and temporally, especially for light precipitation rates and snow-covered or cold surfaces, inhibiting the use of emission-based channels. Light rainfall also presents a problem to spaceborne precipitation radar technology. The lightest precipitation detectable by the TRMM PR, for example, is ~0.7 mm h^{-1} (more or less independent of surface type), assuming a Z-R relationship appropriate to tropical precipitation and that the entire 4 km footprint of the PR is filled with rain (Iguchi et al., 2000). Thus, while current rainfall sensors likely capture a majority of the moderate to heavy precipitation that dominates the Tropics, a significant fraction of lighter precipitation at higher latitudes may be missed. This point is illustrated in Fig. 1, which presents the fractions of zonally averaged precipitation accumulation that falls in the form of liquid precipitation lighter than 1 mm h^{-1} and snowfall derived from the Comprehensive Ocean-Atmosphere Data Set (COADS) ship-borne meteorological observations between 1958 and 1991. While this dataset is by no means intended to represent the true zonal distribution of these types of precipitation, it does suggest that a significant fraction of the precipitation that falls at latitudes poleward of 30^{o} and, in turn, a large fraction of the fresh water in these regions derives from forms of precipitation that are near or below the thresholds of detection of these instruments. Regrettably, for light precipitation over the global oceans there is scant and

incomplete validation data from which to quantify how much of the rain distribution we are effectively capturing. This paper provides an overview of the anticipated role CloudSat (Stephens et al, 2002) observations may play in quantifying the global distribution of light rainfall and its variability on synoptic and seasonal timescales providing a unique opportunity to study their role in global climate change.

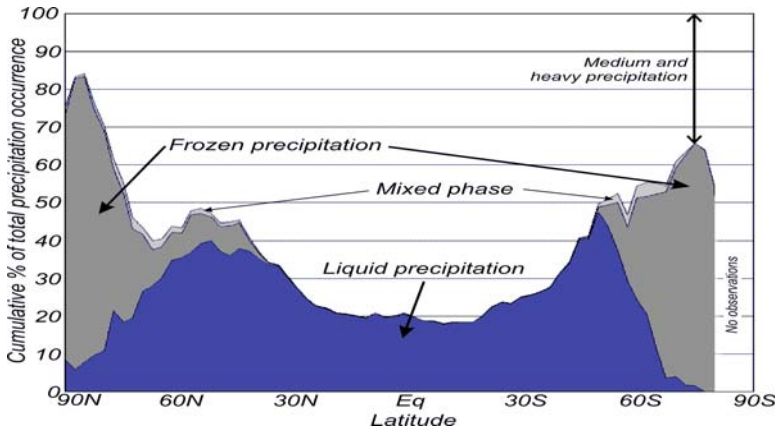

Figure 1: Frequency of occurrence of light rainfall (less than 1 mm h^{-1}) and snowfall from the COADS dataset (courtesy C. Kidd).

2. CLOUDSAT'S NEW PERSPECTIVE

CloudSat and the Cloud-Aerosol Lidar and Infrared Pathfinder Satellite Observations (CALIPSO) satellites were successfully launched from Vandenberg Air Force Base in California on April 26, 2006. Shortly thereafter these satellites joined Aqua in a sun-synchronous orbit at an altitude of 705 km with an equatorial crossing time of 1:30 pm local time in the ascending mode of their orbits. From the moment it was activated on May 20, 2006, the 94 GHz CloudSat Cloud Profiling Radar (CPR) has provided an unprecedented view of the vertical structure of clouds around the planet. From the very beginning, the CPR has also provided a unique perspective on light precipitation around the planet as evidenced by Figure 2 that depicts the first image acquired by CloudSat. The upper panel illustrates that the observations were acquired over the North Sea while the lower panel presents a 1300 km vertical cross section of observed radar reflectivity for this segment. The image clearly depicts a variety of high and low clouds along with a large (~200 km) precipitation feature that extends from the surface to about 10 km in height. While Figure 2 does not in any way present quantitative retrieval results, this first image acquired by the CPR provided strong motivation for developing the rainfall products for CloudSat that will be described in Sections 3 and 4. Other images like these (eg. Figure 6) provided evidence of CloudSat's sensitivity to frozen precipitation further motivating the development of a quantitative snowfall retrieval algorithm that is currently underway.

3. RAINFALL DETECTION WITH CLOUDSAT

3.1 PATH-INTEGRATED ATTENUATION APPROACH

While the strong attenuation is often considered a drawback to precipitation retrieval at shorter radar wavelengths, it can provide a useful measurement for the purpose of rainfall detection. In particular, given suitable assumptions regarding the raindrop size distribution (DSD), the path-integrated attenuation (PIA) can be directly related to the rainfall intensity. This PIA-based method for identifying rainfall forms the basis of CloudSat's rainfall dectection product and will form the early rainfall statistics described here.

To measure PIA, one must first establish the characteristics of the surface backscatter signal under clear-sky conditions. The PIA then follows as the difference between this clear-sky return and that observed by the satellite when precipitation is occurring. Using cloud-masked scenes from CloudSat's first 6 months in

orbit, a database of surface backscatter was developed over the global oceans. Analysis of this dataset reveals that the backscatter of the ocean surface may be determined to a high degree of accuracy from the surface wind speed and sea surface temperature (SST). Using surface winds retrieved by the nearly co-located AMSR-E instrument and SST derived from the NOGAPS model, a model for the clear-sky surface backscatter as a function of these two variables has been developed.

In principle, then, to determine whether a given oceanic CloudSat pixel is raining, the PIA is first determined by differencing the observed surface backscatter from theoretical clear-sky value and if the difference exceeds the standard deviation in the clear-sky surface return (i.e. the noise) the pixel is assumed to be precipitating. In practice, however, it is useful to apply some additional checks to improve the quality of the rainfall product. When PIA exceeds an assumed threshold, taken to be 20 dB, rain is nearly certain to be occurring. Below this threshold, where the radar signal is unlikely to be completely attenuated by heavy rainfall, the value of the reflectivity in the lowest clutter-free bin above the surface is used as an additional constraint to identify scenes that are raining (Z > 0 dBZ), possibly raining (Z > -7 dBZ), or probably not raining (Z < -7 dBZ). Finally, for pixels that are determined to contain precipitation, the observed PIA is related to rainfall intensity assuming a Marshal-Palmer distribution of rain drops and the observed cloud boundaries.

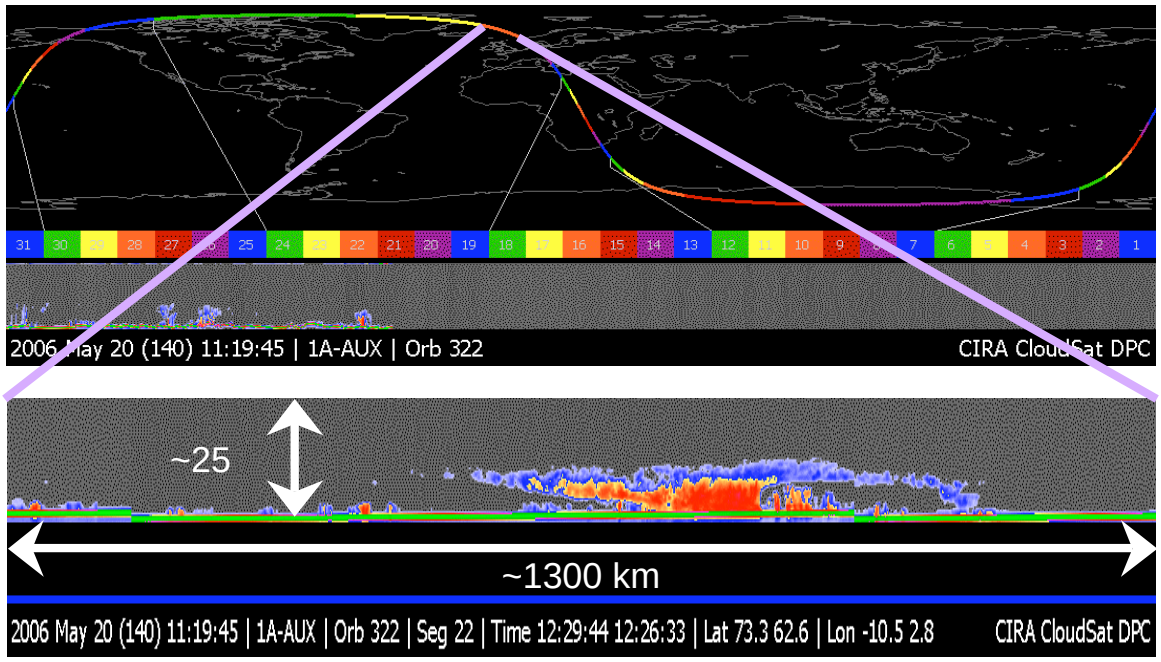

Figure 2: CloudSat's "first image" acquired May 20, 2006 (adapted from the CloudSat Data Processing center website http://cloudsat.cira.colostate.edu).

3.2 COMPARING RAINFALL STATISTICS AGAINST AMSR-E

It has already been noted above that the nature of the PMW rainfall signature poses a challenge at in light precipitation due to the difficulty associated with discriminating cloud from rain. This is particularly true when the freezing level is low and the vertical extent of the liquid water is shallow. The low horizontal resolution of PMW sensors also lead to uncertainty in rainfall estimates in scenes with significantly variable precipitation. By virtue of its 240m vertical and 1.4 km horizontal resolution, the CPR offers an opportunity to examine rainfall systems at a much higher resolution than afforded by PMW sensors. In addition, it's strong sensitivity to particle size, particularly in very light precipitation, makes CloudSat an ideal sensor for

accurately determining precipitation occurrence. On the other hand, this high sensitivity to drop size can lead to large uncertainties in rainfall intensity. It is, therefore, of great interest to exploit the coincident observations of CloudSat and the AMSR-E instrument aboard Aqua in an effort to better understand the magnitudes of the dominant sources of uncertainty suffered by each.

Preliminary comparisons of rainrate histograms from carefully matched CPR and AMSR-E observations are presented in Figure 3 for the two-month period from July 10, 2006 through September 11, 2006. Two regions are highlighted consisting of the zonal belt between 10ºN and 10ºS and another from 40ºS and 60ºS to contrast tropical precipitation with that found at higher latitudes in winter. While very preliminary in nature and covering only a very short duration, even these initial rainfall PDFs illustrate the challenges faced by PMW sensors at higher latitudes. The sensors agree reasonably well in the tropics with AMSR-E retrieving slightly more light rainfall and CloudSat retrieving a number of heavier events consistent with the higher spatial resolution of the latter. Between 40ºS and 60ºS, however, where the freezing level is typically between 1 and 2 km at this time of year, the AMSR-E identifies significantly fewer rainfall events than CloudSat, presumably due to the LWP threshold used for rain/no-rain discrimination. While no rigorous conclusions should be drawn from these early results, they do point to a potentially valuable contribution that CloudSat observations may make in assessing the rainfall discrimination capabilities of PMW sensors. Further processing of the full year of CloudSat data that have been collected to date may help shed more light on the detection capabilities and limitations of both sensors.

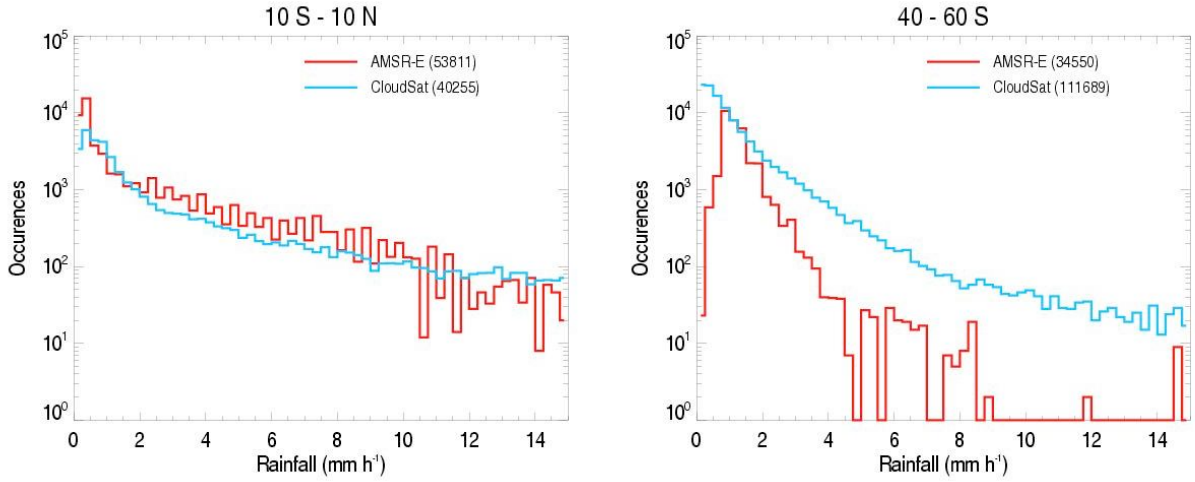

Figure 3: Preliminary comparison of rainfall statistics from CloudSat (red) and the AMSR-E instrument aboard Aqua (red). Statistics in two 20º zonal belts are shown: one centered on the equator (left) and the other from 40-60ºS.

3.3 GLOBAL DISTRIBUTIONS

Global distributions of precipitation occurrence for the same period are presented in the upper panels of Figure 4 for both sensors. At first glance the distributions of rainfall incidence measured by AMSR-E and CloudSat appear very similar showing maxima in regions of persistent large-scale convergence and minima in several well-defined subsidence regions. There are, however, some important differences. Most notably, CloudSat data suggest that precipitation is significantly less frequent in the mid-latitude storm tracks than indicated by the AMSR-E. Conversely, CloudSat occasionally encounters small areas of light precipitation in some of the subsidence regions that is not captured in the AMSR-E products. The differences between the products is even more pronounced when the results are further stratified by precipitation intensity. The remaining panels of Figure 4 show the fraction of precipitation events coming from very light, light, and moderate to heavy precipitation defined as being less than 1 mm h^{-1}, between 1 and 5 mm h^{-1}, and greater than 5 mm h^{-1}, respectively. The results clearly demonstrate the differences in algorithm physics between

the two sensors. CloudSat, for example, indicates that a larger fraction of the precipitation in subsidence regions comes from the 1-5 mm h^{-1} category presumably due to its much higher spatial resolution relative to the AMSR-E that may smooth out these narrow shallow convective cells over it's much larger footprint, yielding lower rainrate estimates. Conversely, AMSR-E observes a much higher frequency of events in the highest rainfall category in the convergence zones. This is likely an artifact of multiple scattering that can contribute significant amounts of spurious reflectivity in heavier rainfall in the CloudSat footprint. This, in turn, artificially increases the observed surface return, decreases the inferred PIA, and therefore aliases higher rainfall rates into the lower rainrate category. It should be noted that an algorithm is being developed for correcting for the effects of multiple scattering using Monte Carlo simulations that explicitly account for higher order scattering events and it is anticipated that this correction will be applied prior to the official release of these products.

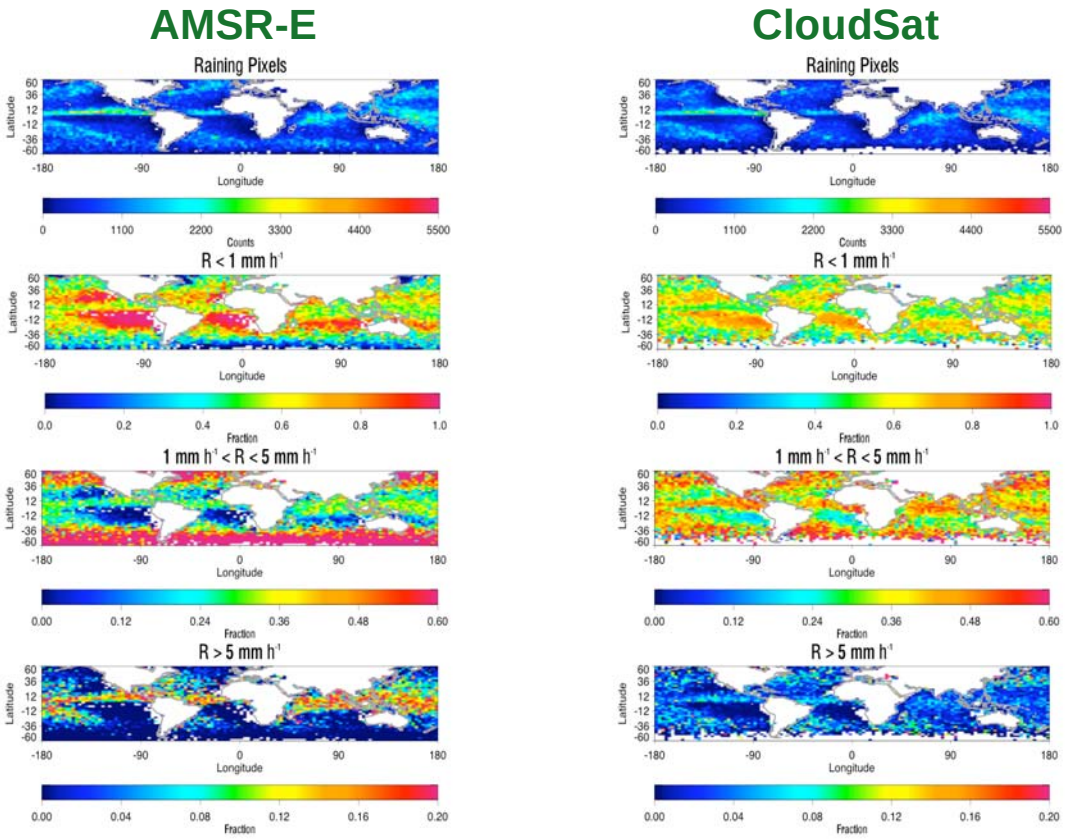

Figure 4: Global distribution of rainfall occurrence (top) between July 10, 2006 and January 18, 2007 from AMSR-E (left) and CloudSat (right). The three remaining panels show the fraction of rainfall occurrence due to rainfall in three different intensity ranges: less than 1 mm h^{-1} (second panel), between 1 and 5 mm h^{-1} (third panel), and greater than 5 mm h^{-1} (bottom panel).

5. TOWARD A COMPLETE RAINFALL PROFILING ALGORITHM

The suite of algorithms developed for CloudSat have been designed to both take advantage of complementary information from the other sensors on the A-Train, such as AMSR-E and MODIS radiance data from Aqua, and to provide rigorously-derived estimates of the uncertainties in each product. Following this mold, the CloudSat light rainfall algorithm has been formulated in the optimal estimation framework (Rodgers, 2000) that explicitly accounts for uncertainties in all sources of input data and propagates these uncertainties through the retrieval physics to supply corresponding estimates of the uncertainties in all retrieved products. In addition, the algorithm has been formulated with the capability of including a precipitation water path constraint from AMSR-E. Due to the strong attenuation of precipitation-sized

hydrometeors at 94 GHz, the rainfall algorithm also requires an integral constraint in the form of the Path Integrated Attenuation (PIA) to unambiguously retrieve rainfall rate. Additional details of the algorithm can be found in L'Ecuyer and Stephens (2002) or L'Ecuyer et al. (2004).

This algorithm has been implemented at the Naval Research Laboratory on its near real-time processing system (NRTPS). The NRTPS was established to handle multisensor (currently, 23 optical and microwave environmental satellite sensors from a constellation of 13-polar orbiting and 6-geostationary platforms) and model fusion (from the Navy global and mesoscale prediction systems) processing within a research and development framework. While NRL's commitment to operational transition of its research deliverables to a great extent necessitates such a system, its benefits extend beyond the facilitation of transition. During Operation Iraqi Freedom, NRL exploited the NRTPS in providing satellite meteorology support (e.g., dust, rainfall, fire, cloud properties, snow, and high resolution true color imagery) directly to DoD and Coalition assets within a timeframe useful for a wide variety of applications that included mission planning, ship navigation, and target/weaponry selection (Miller et al., 2005). Level-1B CPR data (calibrated cloud reflectivity) are ingested within an average of 6 hrs of being collected enabling the staging of these data upon the NRPTS with the full complement of contemporary satellite/model digital datasets. The retrieval is performed on all pixels determined to be cloudy by the CloudSat geometric profile product (GEOPROF) that is run as a preprocessing step. Ancillary data (e.g., global temperature/moisture profiles, surface winds, and surface temperatures) are supplied from the Navy Operational Global Atmospheric Prediction System (NOGAPS). These data are used to compute the component of attenuation due to atmospheric gaseous absorption as well as to define the surface wind speed needed to estimate the expected clear-sky surface return required to estimate PIA.

An example of a rainfall retrieval from a precipitation system off the coast of South Carolina is shown in Figure 5. The scene consists of several rain bands with embedded convective cores between 10 and 15 km deep two of which were intersected by CloudSat. The CloudSat reflectivity cross-section indicates a smaller developing convective cell on the left followed by a larger area of more mature precipitation characterized by thick cirrus cloud overlying a persistent area of moderate rainfall with a well-defined melting level at ~4.5 km. Reflectivities exceeding 10 dBZ throughout most of the scene indicate the presence of large precipitating liquid and ice particles and the decrease in reflectivity in the rainfall between the melting level and the surface is indicative of their strong attenuation at 94 GHz. Retrieved surface rainfall rate for the indicated region is presented on the right and compared with similar estimates from the NEXRAD data themselves. Retrieved rainrates range from less than 1 to above 10 mm h^{-1} across the scene and those from CloudSat (black curve) generally agree with those from the ground radar to within the uncertainty expected from using three different standard NEXRAD Z-R relations that may be appropriate for this region (colored curves). Subtle differences in the precise location and magnitude of intensity peaks may also be a result of imperfect time/space matching of the two datasets as well as differences in the sample volumes of the two instruments. While this in no way guarantees that the CloudSat rainfall estimates are quantitatively accurate, it provides a reassuring sanity check that the results are in line with those obtained by more traditional precipitation sensors and further motivates the generation of a standard CloudSat light rainfall product. This example also serves to illustrate the fact that despite the strong attenuation at 94 GHz, CPR observations may be capable of retrieving rainfall out to higher intensities than previously thought. Here the CloudSat algorithm is capable of capturing rainfall rates exceeding 10 mm h^{-1} with no sign of degradation due to the corresponding attenuation provided it is modeled correctly.

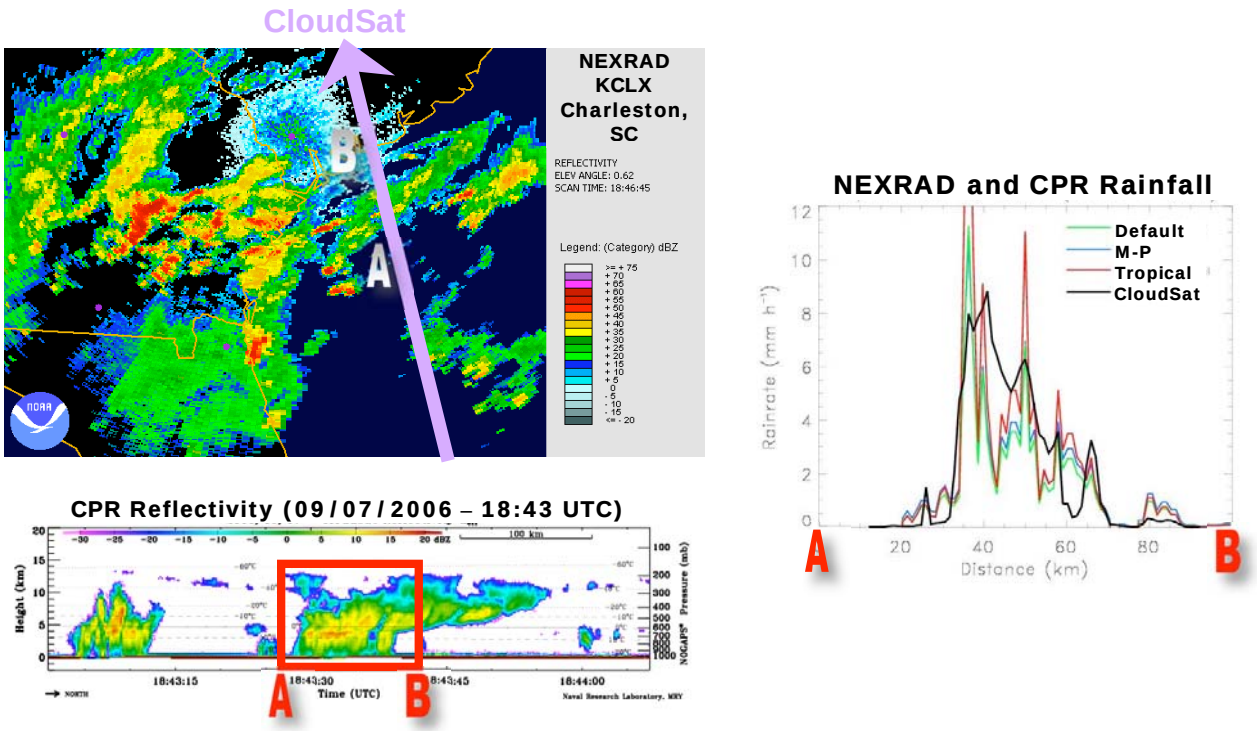

Figure 5: Early rainfall retrieval from CloudSat. The upper left hand panel shows the lowest scan of the Charleston NEXRAD radar (KCLX) with the CloudSat ground track superimposed. The lower left hand panel shows corresponding reflectivities observed by the CPR. The panel on the right shows retrieved rainfall from CloudSat (black curve) along with three different rainfall estimates from the NEXRAD radar derived using three distinct Z-R relationships.

7. DISCUSSION

Early results from the application of two new light rainfall algorithms to data acquired during CloudSat's first year of operation confirm its potential for quantifying the role played by light rainfall in the global water cycle. It is important to emphasize that neither of these algorithms has undergone any formal validation but it is encouraging that the results are reasonable given the regions examined and time of year. With the growing amount of field data being acquired in support of CloudSat's validation program, extensive evaluation of both the rainfall occurrence and intensity estimates from these algorithms are ongoing. It is anticipated that these products will continue to be refined and improved in the coming year and will ultimately form the basis of enhanced science products for the CloudSat mission that will be made available to the science community through the CloudSat Data Processing Center (http://www.cloudsat.cira.colostate.edu/dpcstatusTrack.php) as early as next year.

Although it is not the primary focus of this paper, snowfall is common during the winter months at the mid and high latitudes and represents a significant fraction of the fresh water used for consumption and agriculture in these regions measuring snowfall from current satellite-based precipitation sensors has been difficult due to challenges associated with distinguishing falling snow from that on the surface. It is, therefore, worth noting that CloudSat reflectivities also provide a means for detecting this snowfall and may allow quantitative retrievals of falling snow particularly when combined with the high frequency (89 GHz) channel of AMSR-E. As an example, a snowfall scene acquired by CloudSat on August 29, 2006 off the coast of Antarctica is shown in Figure 6. The scene consists of a widespread area of variable snowfall approximate 400 km long just off the coast of Antarctica (note the coast can just been seen on the far right hand side of the bottom of the lower panel of Figure 6 depicted in brown). Reflectivities range from 0-10

dBZ and the cloud layer ranges in thickness from 2-5 km with evidence of some relatively heavy snow bands embedded in the system.

Quantitative snowfall rate estimates are complicated by the numerous governing crystal shape, size distribution, density, and melted fraction and are, therefore, beyond the scope of the present study. The PIA-based detection algorithm described in Section 3.1 has, however, been augmented to use a combination of PIA, reflectivity, and ECMWF 2 m air temperature to discriminate rainfall and snow at the surface. A preliminary estimate of the zonal mean frequency of occurrence of both rainfall and snowfall from CloudSat is presented in Figure 7 for the period from July 2006 – January 2007. To our knowledge these results represent the first attempt to quantify the global distribution of snowfall occurrence and serve to illustrate the potential for using CloudSat measurements to detect snowfall and possibly even quantify its intensity on the global scale although the latter remains a topic for future study.

The over-arching goal of the A-Train constellation is to provide a synergistic view of the primary components of the global hydrologic cycle and energy budget including water vapor, clouds, rainfall, aerosols, and the distribution of various chemical species in the atmosphere as well as longwave and shortwave radiative fluxes at the top of the atmosphere. In this broader context, CloudSat's rainfall products open up a number of avenues for further research related to the combination of information from complementary sensors in the constellation. While CloudSat's primary role in the A-Train will continue to be as a source of information concerning the vertical distribution of liquid and ice water content, the ability of the CPR to simultaneously detect liquid clouds, ice clouds, light liquid rainfall, and snowfall will offer insight into processes of fundamental importance to understanding the role of clouds and light precipitation in the large-scale environment. Of particular interest from a climate perspective are the mechanisms for rainfall formation, the processes by which aerosols modify clouds and precipitation, and the resulting implications for the global energy and water cycle. The products introduced here in combination with those from other A-Train sensors, therefore, have the potential to both improve our ability to predict the weather and advance our understanding of several key climatic processes.

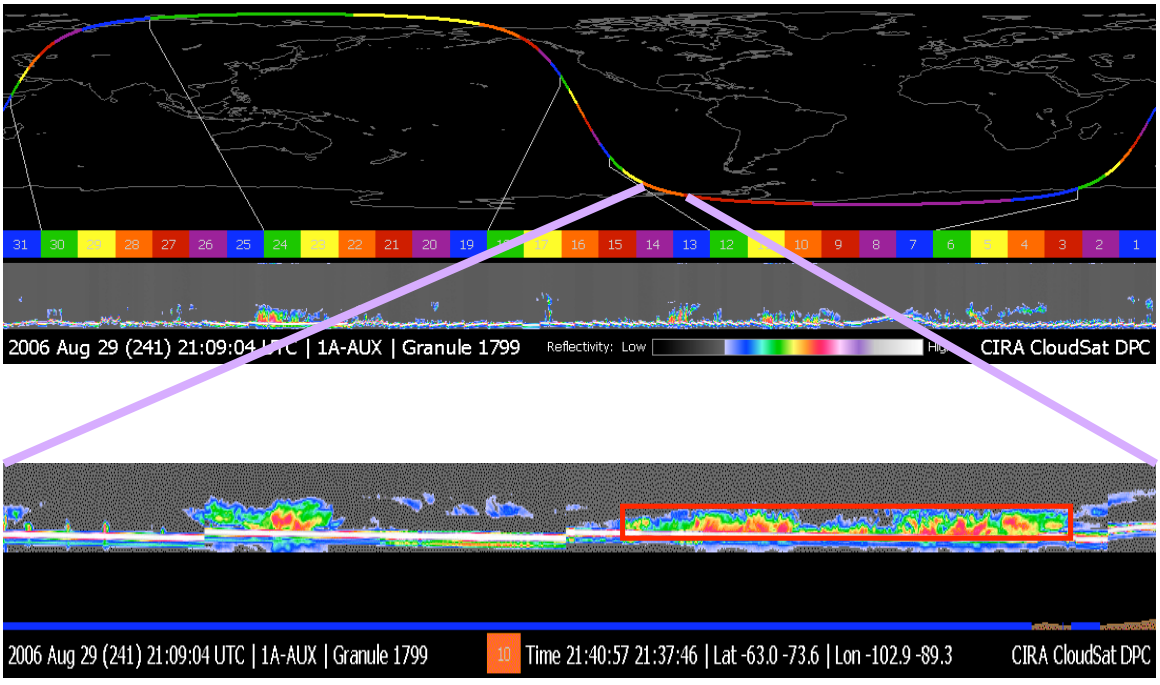

Figure 6: A snowfall scene observed by CloudSat off the coast of Antarctica.

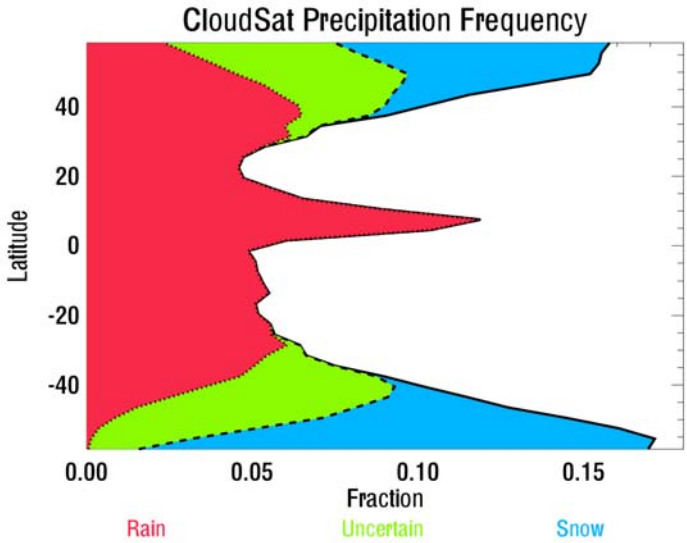

Figure 7: Preliminary zonal rainfall and snowfall occurrence statistics from July 10, 2006 through January 18, 2007 based on CloudSat path-integrated attenuation and reflectivity measurements. Red corresponds to rainfall, blue is snowfall, and the green bar represents scenes for which precipitation phase could not be discriminated unambiguously including mixed-phase precipitation.

8. REFERENCES

L'Ecuyer, T. S. and G. L. Stephens, 2002: An estimation-based precipitation retrieval algorithm for attenuating radars, *J. Appl. Meteor.* **41**, 272-285.

L'Ecuyer, T. S., 2004: Experimental light rainfall and snowfall products for CloudSat, *2nd International Precipitation Working Group Workshop on Precipitation Measurements*, Monterey, CA, 298-305.

Miller, S. D. and co-authors 2006: MODIS provides a satellite focus on Operation Iraqi Freedom, *Int. J. Rem. Sens.* **27**, 1285-1296.

Rodgers, C. D., 2000: Inverse methods for atmospheric sounding. Theory and practice., World Scientific, Singapore, 2000.

Stephens, G. L. and co-authors, 2002: The CloudSat mission and the A-Train: A new dimension of space-based observations of clouds and precipitation, *Bull. Amer. Meteor. Soc.* **83**, 1771-1790.